Journal of NeuroVirology, 8: 420–431, 2002
 ISSN 1355–0284/02 $12.00+.00
DOI: 10.1080/13550280290100851

Neurovirulence depends on virus input titer in brain in feline immunodeficiency virus infection: Evidence for activation of innate immunity and neuronal injury

JB Johnston,[1] C Silva,[1] T Hiebert,[2] R Buist,[2] MR Dawood,[3] J Peeling,[2] and C Power[1]

[1]*Department of Clinical Neurosciences, University of Calgary, Calgary, Alberta, Canada; Departments of* [2]*Radiology and* [3]*Medical Microbiology, University of Manitoba, Winnipeg, Manitoba, Canada*

Lentiruses cause neurological disease depending on the virus strain and its neurotropism, yet it remains uncertain to what the impact of infectious virus quantity in the brain early in infection is on the subsequent development of neurological disease or neurovirulence. We investigated the relationship between infectious virus input titer and the resulting neurovirulence, using *ex vivo* and *in vivo* assays of feline immunodeficiency virus (FIV)-induced neurovirulence. FIV infection of cell cultures and neonatal cats was performed using $10^{2.5}$ (low-titer) or $10^{4.5}$ (high-titer) 50% tissue culture infectious doses ($TCID_{50}$)/ml of the neurovirulent FIV strain, V1CSF. *Ex vivo* neurotoxicity assays revealed that conditioned medium (CM) from feline macrophages infected with high-titer ($P < .001$) or low-titer ($P < .01$) V1CSF induced greater neuronal death than CM from mock-infected cells. *In vivo*, animals infected intracranially with high-titer V1CSF showed neurodevelopmental delays compared to mock-infected animals ($P < .001$) and animals infected with low-titer V1CSF ($P < .02$), concurrent with reduced weight gains and greater depletion of $CD4_+$ cells over a 12-week period. Neuropathological changes, including astrogliosis, macrophage activation, and neuronal damage, were evident in V1CSF-infected animals and were viral titer dependent. *In vivo* magnetic resonance (MR) spectroscopy and proton nuclear magnetic resonance (^{1}H-NMR) spectroscopy of tissue extracts revealed evidence of neuronal injury, including reduced *N*-acetyl aspartate/creatine ($P < .05$) and increased trimethylamine/creatine ($P < .05$) ratios, in the frontal cortex of high-titer V1CSF-infected animals compared to the other groups. T2-weighted MR imaging detected increased signal intensities in the frontal cortex and white matter of V1CSF-infected animals relative to controls, which was more evident as viral titer increased ($P < .01$). The present findings indicate that lentivirus infectious titers in the brain during the early stages of infection determine the severity of neurovirulence, reflected by neurobehavioral deficits, together with neuroradiological and neuropathological findings of activation of innate immunity and neuronal injury. *Journal of NeuroVirology* (2002) **8,** 420–431.

Keywords: feline immunodeficiency virus; MR spectroscopy and imaging; neurotoxicity; neurovirulence; viral titer

Introduction

Feline immunodeficiency virus (FIV) is a lentivirus that causes immunological and neurological impairment in domestic cats similar to that seen in human immunodeficiency virus (HIV)-infected patients (Bendinelli *et al*, 1995). Like HIV, FIV is neurotropic, entering the central nervous system (CNS) during the early stages of infection and primarily infecting microglia and astrocytes (Dow *et al*, 1992).

Address correspondence to Dr. C Power, Department of Clinical Neurosciences, HMRB 150, 3330 Hospital Dr., NW, University of Calgary, Calgary, Alberta, Canada T2N 4N1. E-mail: power@ucalgary.ca

The authors thank Colleen Geary for animal care assistance. The Canadian Institutes of Health Research, the Natural Sciences and Engineering Research Council of Canada, and CANFAR supported these studies. JBJ is an AHFMR Student and CP is an AHFMR Scholar/CIHR Investigator.

Received 14 March 2002; revised 25 June 2002; accepted 9 July 2002.

In twenty percent to forty percent of FIV-infected felines, invasion of the CNS is associated with neurological abnormalities that manifest as FIV encephalopathy (FIVE). FIVE presents as neurobehavioral abnormalities such as psychomotor slowing, ataxia, aggressivity, disrupted sleep and arousal patterns, stereotypic motor behaviors, and altered sensory evoked potentials (reviewed in Podell *et al*, 2000). Although overt clinical signs of neurological disease are not always observed, neuropathological changes, such as neuronal injury and loss, inflammation, microglial nodules, white matter pallor, and gliosis, are apparent in many FIV-infected cats upon necropsy (Hurtrel *et al*, 1992; Phillips *et al*, 1994).

The events that contribute to the development of FIVE remain unclear, but as with the primate lentiviruses, neuronal damage in the absence of productive infection of neurons by FIV suggests an indirect mechanism (Power, 2001). Consequently, infection and activation of glia and brain macrophages has been posited to result in the increased expression of putative neurotoxins, including both viral proteins (Billaud *et al*, 2000; Bragg *et al*, 1999; Gruol *et al*, 1998) and host-derived molecules, such as proteolytic enzymes and proinflammatory cytokines (Johnston *et al*, 2000; Poli *et al*, 1999; Zenger *et al*, 1997). Ultimately, neuronal death is thought to involve an excitotoxic mechanism resulting from dysregulation of calcium exchange or neurotransmitter uptake and release (Billaud *et al*, 2000; Bragg *et al*, 1999; Gruol *et al*, 1998; Yu *et al*, 1998). The potential for the interplay between virus and host factors to influence disease progression is exemplified further by the relationship between viral burden and neurovirulence. For example, the neurological damage induced by lentiviruses may occur early in infection when plasma viral load is high yet the host immune response is still intact in both humans and animals infected by lentiviruses (Boche *et al*, 1996; McArthur, 1987). However, neurological complications are most apparent during the advanced stages of disease when viral load is again elevated concurrent with a diminished immune response (Boche *et al*, 1996), suggesting that the extent of viral replication within the CNS, and factors that influence this process, determine the extent of neurological damage caused by lentiviruses. In support of this concept, systemic immune suppression has been shown to be an important determinant of FIV neurovirulence (Podell *et al*, 1997; Power *et al*, 1998). Furthermore, an association between FIV replication in the brain and the induction of proinflammatory cytokines, such as tumor necrosis factor alpha (TNF-α), has been reported (Poli *et al*, 1999).

Although a strong correlation has been reported between cerebrospinal fluid (CSF) viral burden and the development of progressive neurological disease following lentiviral infection (Boche *et al*, 1996; McArthur *et al*, 1997; Zink *et al*, 1999), the relationship between brain viral load and neuropathogenesis remains unresolved. Moreover, little is known about how brain viral burden early in infection influences the subsequent development of neurological disease. In the present study, we examined the extent to which input titer in the brain influenced the neurovirulence exhibited by the primary FIV isolate, V1CSF, in a neonatal feline model of neurological impairment. An input titer-dependent response was observed between V1CSF titer and the resulting neuropathology and neurodevelopmental impairment, together with concomitant neuroradiological and systemic immune abnormalities.

Results

Ex vivo *neurotoxicity induced by V1CSF*

Because the release of neurotoxins by infected and/or activated macrophages has been posited to contribute to the neuronal injury induced by FIV (Zenger *et al*, 1997), primary feline monocyte-derived macrophages (MDM) were infected with V1CSF and conditioned medium (CM) harvested at days 1 and 3 post infection (PI). Neurotoxicity was determined by treating differentiated NG108 cells with CM for 24 h and assessing cell death by trypan blue exclusion. Neuronal death relative to untreated cultures and cultures treated with CM from mock-infected MDM was increased following incubation with CM harvested from MDM infected with either high ($P < .001$) or low ($P < .01$) titers of V1CSF (Figure 1). Although

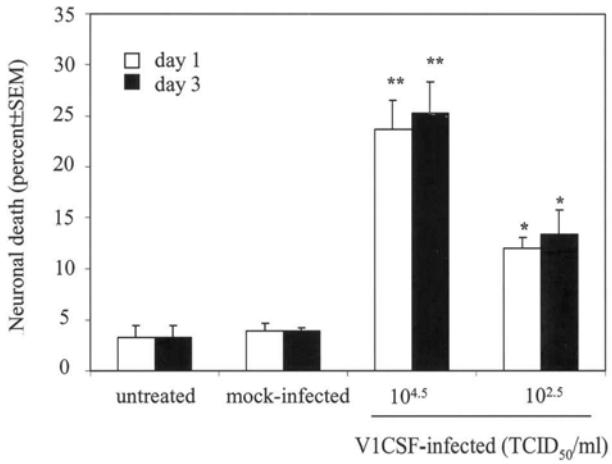

Figure 1 *Ex vivo* neurotoxicity exhibited by V1CSF is titer-dependent. Primary feline MDM were mock-infected or infected with $10^{2.5}$ or $10^{4.5}$ $TCID_{50}$/ml of V1CSF and CM harvested at days 1 and 3 PI. Differentiated NG108 neuroblastoma cells were incubated with CM for 24 h and cell death, equalized for the total number of cells, was determined by trypan blue exclusion. Cells incubated with fresh medium (untreated) served as controls for background neurotoxicity. Results represent the mean ± SEM (percent total cells) of trypan blue–positive cells detected in three wells (4 fields/well). Significant differences relative to neurons treated with CM from mock-infected MDM were determined by ANOVA and Tukey-Kramer post hoc tests ($^{**}P < .001$; $^{*}P < .01$). Greater neurotoxicity was observed at both days with CM from MDM infected with $10^{4.5}$ $TCID_{50}$/ml of V1CSF compared to cells infected with $10^{2.5}$ $TCID_{50}$/ml.

neurotoxicity did not differ between cultures incubated with media harvested at day 1 or 3 PI, differences were detected depending on the viral titer with which MDM were infected. CM harvested from MDM infected with high viral titers caused levels of cell death (approximately 25%) that were increased significantly ($P < .001$) compared to levels caused by CM from MDM infected at low titers (approximately 13%). Thus, the capacity for V1CSF to induce the release of potential neurotoxins from infected MDM *in vitro* was dependent on viral input titer.

Systemic effects of V1CSF infection

To assess the influence of viral titer on FIV infection *in vivo*, neonatal kittens were mock-infected or inoculated with either $10^{2.5}$ (low-titer) or $10^{4.5}$ (high-titer) 50% tissue culture infectious doses ($TCID_{50}$)/ml of V1CSF by intracranial injection and followed over a 12-week period. Systemic infection was confirmed by reverse transcriptase–polymerase chain reaction (RT-PCR), which detected FIV-specific sequences in peripheral blood mononuclear cells (PBMC) harvested at weeks 8 and 12 PI from all infected animals, but not in cells from mock-infected controls (data not shown). Analysis by flow cytometry of PBMC isolated at week 8 PI from V1CSF- and mock-infected cats revealed no significant differences in the percentage of CD4+ cells between groups (12% to 15%) (Figure 2**a**). In contrast, CD4+ cell levels were significantly lower at week 12 PI ($P < .001$) in animals infected with either titer of V1CSF compared to mock-infected cats. These differences reflected an increase in the number of CD4+ cells in control animals (80%), whereas levels decreased by 50% and 18% in high-titer and low-titer V1CSF-infected animals, respectively. Comparison of CD8+ cells at the same time points indicated that levels were increased significantly in both V1CSF-infected groups compared to controls at week 8 PI ($P < .001$), but at week 12, only CD8 levels in low-titer animals differed from controls (Figure 2**b**). Over this period, the abundance of CD8+ cells increased in both control (150%) and low-titer (66%) animals, but remained unchanged in high-titer cats. Taken together, these results indicated that input viral titer had the capacity to influence the extent of systemic disease characterized by immunosuppression.

Weekly determinations of body weights indicated that progressive weight gains occurred in both mock- and FIV-infected animals (Figure 2**c**). However, after 2 weeks PI, the mean weights of high-titer neonates were significantly lower than those of controls ($P < .005$ at weeks 4, 6, and 8; $P < .05$ at weeks 10 and 12), whereas differences between low-titer and mock-infected animals were not observed until week 10 PI ($P < .05$ at weeks 10 and 12). Similarly, animals receiving high-titers of V1CSF exhibited decreased weight gains compared to low-titer neonates until week 10 PI ($P < .05$ at weeks 4, 6, and 8).

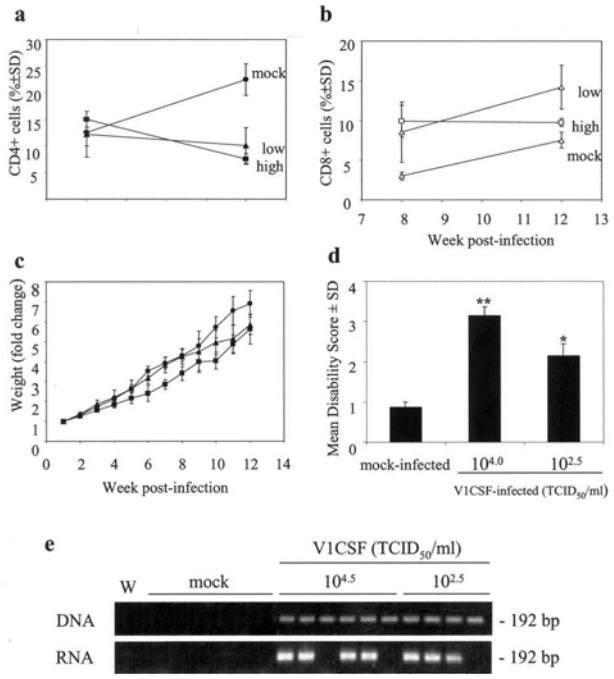

Figure 2 Systemic and neurobehavioral changes in V1CSF-infected neonates. (**a**) Neonatal cats were mock-infected ($n = 7$) or infected intracranially with high ($10^{4.5}$ $TCID_{50}$/ml; $n = 6$) or low ($10^{2.5}$ $TCID_{50}$/ml; $n = 4$) titers of V1CSF. (**a**, **b**) PBMC were isolated from whole blood collected at weeks 8 and 12 PI and the number of CD4+ (**a**) and CD8+ (**b**) cells determined by flow cytometry. Results are expressed as the mean percentage ± SD of labeled cells relative to the total number of PBMC. CD4 levels in cats infected with high-titer V1CSF were significantly decreased compared to mock-infected ($P < .001$) and low-titer ($P < .05$) animals at week 12 PI. CD8 levels were originally increased in both V1CSF-infected groups relative to controls at week 8 PI ($P < .001$), but increased in mock-infected and low-titer animals and decreased in cats infected with high-titer V1CSF between weeks 8 and 12 PI. (**c**) Weight changes relative to the starting weight (week 1) assessed for each animal. Decreased weight gains compared to mock-infected cats were evident after week 2 in animals infected with high-titer V1CSF ($P < .005$ at weeks 4, 6, and 8; $P < .05$ at weeks 10 and 12) and after week 8 in animals infected with low-titer V1CSF ($P < .05$). Weight gains by high-titer cats were also significantly less than those of low-titer animals before week 10 PI ($P < .05$). (**d**) Developmental parameters (play interaction, walking, running, jumping, air righting, blink reflex, plank walking) were measured weekly for 12 weeks in the mock- and V1CSF-infected neonates. Neurodevelopmental impairment was scored based on the mean age (weeks) at which animals in each group were able to successful complete a given task and results expressed as the mean disability score (MDS) ± SD for each group. Compared to controls, the neurobehavioral development of animals infected with either high-titer or low-titer V1CSF was significantly delayed, with high-titer animals exhibiting a greater degree of impairment than low-titer animals. (**e**) Necropsied brain (frontal lobe) tissue was obtained at 12 weeks PI from mock- and V1CSF-infected the presence of the FIV *pol* gene in genomic DNA and cDNA confirmed by nested PCR analysis. Representative gels are shown for four animals in each group. A water blank (W) served as a contamination control. Viral DNA was detected in all V1CSF-infected animals, but not in mock-infected controls. However, FIV RNA was detectable only sporadically in infected neonates. Significant differences relative to mock-infected animals were determined by Student's *t* test ($^{*}P < .05$; $^{**}P < .001$). Data represent the mean ± SD for each group, with significant differences determined by ANOVA and Tukey-Kramer post hoc tests.

Neurodevelopmental impairment and virus detection in V1CSF-infected neonates

To assess the role of viral titer in the development of neurological disease following FIV infection, a feline model of neurodevelopmental impairment reported previously (Power *et al*, 1998) was used. Compared to mock-infected controls, which had a mean disability scale (MDS) score of 0.9 ± 0.1, animals infected with either high or low titers of V1CSF exhibited developmental delays (Figure 2**d**). However, the level of impairment in high-titer animals (3.2 ± 0.2) was significantly greater ($P < .02$) than that observed for low-titer cats (2.2 ± 0.6). Furthermore, no differences were observed in the development of neurological disease when animals from different litters were infected with the same viral titer. To confirm infection and the presence of viral replication in the brain, nested PCR and RT-PCR analysis of mock- and V1CSF-infected brain tissue was performed. PCR analysis of genomic DNA revealed the presence of FIV sequences at week 12 PI in brain tissue collected at necropsy from all infected animals, but FIV was not detected in brain samples from any of the controls (Figure 2**e**). In contrast, FIV sequences were detected in only four of six high-titer and three of four low-titer V1CSF-infected animals following RT-PCR amplification.

V1CSF infection is associated with gliosis and neuronal stress

The morphological changes associated with the neurological impairment observed in the FIV-infected neonates were investigated by immunocytochemical analysis of serial sections of necropsied frontal lobe from mock-infected animals and cats infected with different titers of V1CSF. Glial fibrillary acidic protein (GFAP) immunoreactivity was increased in the brains, chiefly in white matter, of high-titer (Figure 3**B**) and low-titer (Figure 3**C**) V1CSF-infected cats, demonstrating astrocyte hypertrophy and an increased number of detectable processes compared to control brains (Figure 3**A**). Similarly, evidence of increased macrophage/microglial activation in infected animals compared to controls was provided by the ability to detect a greater number of cells immunopositive for CD18, which labels monocytoid cells (macrophages/microglia) and lymphocytes (Figure 3**D–F**). However, the extent of astrogliosis and macrophage activation were increased in animals infected with high titers of V1CSF compared to low-titer cats. Immunostaining with antibodies to microtubule-associated protein (MAP)-2 (Figure 3**G–I**) did not reveal obvious neuronal loss in any V1CSF-infected group, although reduced neuronal processes and dysmorphic neurons were observed in the high-titer group (Figure 3**H**). Evidence of neuronal stress, such as increased immunoreactivity to the transcription factor *c-fos* (Figure 3**J–L**), was detected in brain tissue from high-titer animals (Figure 3**K**), compared to low-titer FIV–infected and control brains. Of note, *c-fos* staining was observed primarily in the nuclei of neurons, with minimal cytoplasmic staining. In addition, a few *c-fos*–positive cells were detected in the low-titer group (Figure 3**L**), but clusters of positive neurons were evident only in animals infected with high titers of V1CSF (Figure 3**K**). It should be noted that consistent with earlier reports from our laboratory (Power *et al*, 1997, 1998), no differences were observed in the severity of neuropathological changes when ipsalateral and contralateral hemispheres were compared.

Magnetic resonance studies

Further evidence of neuronal injury following FIV infection was obtained by magnetic resonance (MR) spectroscopy analysis of brain metabolite levels in mock- and FIV-infected cats. Spectra (Figure 4**b**) were obtained from voxels in the left frontal cortex (Figure 4**a**) or caudate nucleus (spectra not shown) at 12 weeks PI, and metabolite levels in each sample were expressed relative to creatine (Figure 4**c**). Comparison of the cortical spectra revealed decreased *N*-acetyl aspartate (NAA)/creatine (Cr) ratios ($P < .03$), shown previously to be a reliable indicator of neuronal integrity (Prichard and Shulman, 1986), in cats infected with high titers of V1CSF compared to mock-infected controls (Figure 4**c**). The level of metabolites containing trimethyl amine (TMA) groups, such as choline, was increased ($P < .03$) in high-titer animals relative to controls (Figure 4**c**). Like decreased NAA, elevated TMA is indicative of cellular damage, such as loss of membrane integrity (Kugel *et al*, 1998). Of note, glutamate (Glu)/Cr ratios, shown previously to be increased in brain tissue from V1CSF-infected adult cats, were reduced significantly ($P < .05$) in neonatal brains following infection with high-titer V1CSF (Figure 4**c**). Similar trends in metabolite levels were observed in brain tissue from cats infected with low-titer V1CSF, but these changes were less prominent than those detected in high-titer animals and did not differ significantly from mock-infected controls. No differences in metabolite levels were detected when the caudate was examined (data not shown). The results obtained by *in vivo* MR spectroscopy were confirmed by *ex vivo* proton MR spectroscopy of necropsied brain tissue (left frontal cortex) harvested at week 12 PI. Again, high-titer animals exhibited decreased NAA/Cr (0.08 ± 0.04, $P < .01$) and Glu/Cr (1.81 ± 0.14, $P < .01$) ratios compared to low titer (NAA/Cr, 0.98 ± 0.05; Glu/Cr, 2.62 ± 0.19) and mock-infected (NAA/Cr, 1.01 ± 0.04; Glu/Cr, 2.29 ± 0.55). However, no significant differences were detected in the levels of other brain metabolites, including formate, taurine, cholines, aspartate, succinate, γ-aminobutyric acid (GABA), acetate, and alanine, among groups.

To characterize regions of potential injury within the brain, T2-weighted MR imaging was performed on mock- and V1CSF-infected cats at week 12 PI

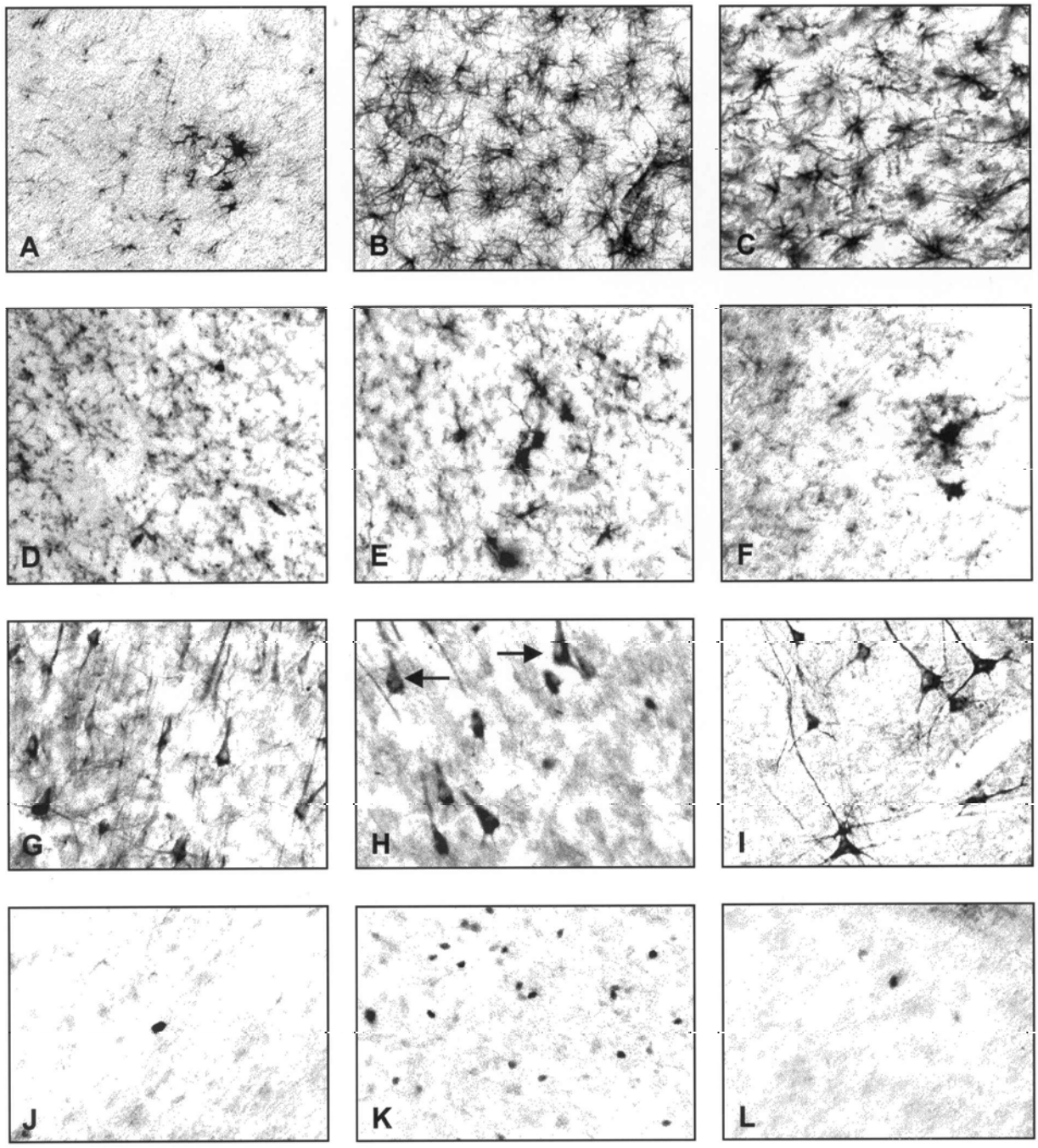

Figure 3 Immunocytochemical analyses of neonatal brain tissue. Serial sections of brain tissue (frontal lobe) collected at 12 weeks PI from mock-infected neonates (**A**, **D**, **G**, **J**) and cats infected with high (**B**, **E**, **H**, **K**) or low (**C**, **F**, **I**, **L**) titers of V1CSF were immunostained with antibodies to GFAP (**A**, **B**, **C**), CD18 (**E**, **F**, **G**), MAP-2 (**H**, **I**, **J**), or *c-fos* (**K**, **L**, **M**). Compared to mock-infected controls (**A**, **D**) and cats infected with low-titer V1CSF (**C**, **F**), GFAP immunoreactivity, indicative of astrogliosis, and levels of CD18-positive activated macrophages were increased in cats infected with high-titer V1CSF (**B**, **E**). Although minimal neuronal loss was observed in V1CSF-infected animals compared to controls, dysmorphic neurons (*arrows*) were more evident in high-titer animals (**H**) compared to the other groups (**G**, **I**). Similarly, increased *c-fos* immunoreactivity, localized primarily to the nuclei of neurons, was detected in neonates infected with high-titers of V1CSF (**K**), compared to isolated, positively stained neurons observed infrequently in controls (**J**) and low-titer animals (**L**). Original magnification, 400× (**A–F**), 200× (**G–L**).

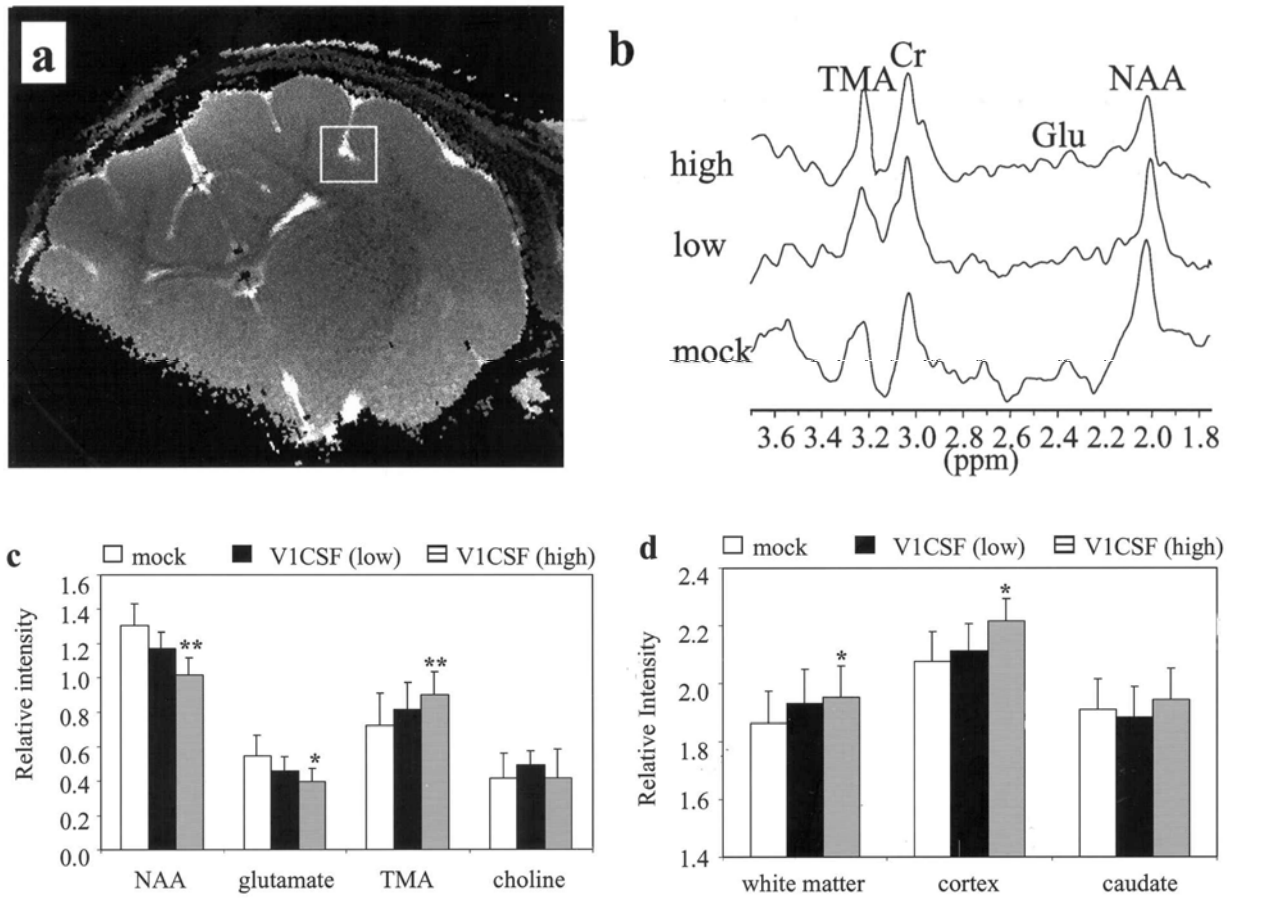

Figure 4 Magnetic resonance (MR) spectroscopy analysis of neonates. (**a**) *In vivo* MR spectroscopy was performed at 12 weeks PI from the mid-frontal sulcus (shown) or the caudate putamen (not shown) of mock-infected animals and animals infected with high or low titers of V1CSF. (**b**) Comparison of representative MR spectra, indicating peaks corresponding to *N*-acetyl acetate (NAA), creatine (Cr), trimethylamines (TMA), and glutamate (Glu). (**c**) The levels of brain metabolites, determined by MR, were normalized to creatine levels and ratios are expressed as the mean ± SD for each experimental group. Compared to controls, the mean NAA/Cr and Glu/Cr were decreased in the cortex of V1CSF-infected animals in a titer-dependent manner. In contrast, cortical TMA/Cr increased with titer in V1CSF-infected animals. Metabolite ratios in the caudate nucleus did not differ between groups (data not shown). (**d**) Titer-dependent increases in T2-weighted signal intensities were observed in frontal cortex and white matter of V1CSF-infected animals compared to mock-infected controls, but not in the caudate nucleus. Values are expressed relative to intensities in muscle from each animal and represent the mean ± SD for each experimental group. Significant differences between groups were determined by ANOVA and Tukey-Kramer post hoc tests ($^{**}P < .01$; $^{*}P < .05$).

and signal intensities, relative to muscle, were determined for the caudate nucleus and left frontal cortex and white matter (Figure 4**d**). Compared to control animals and low-titer–infected animals, higher signal intensities were detected in frontal white matter ($P < .005$) and cortex ($P < .005$) of neonates infected with high-titer V1CSF. Moreover, cortical atrophy was also observed in both low-titer and high-titer FIV–infected animals compared to uninfected controls. Although signal intensities in these regions were elevated slightly in low-titer FIV–infected cats, levels were not significantly increased over control values. In contrast, as with the brain metabolite levels, no differences in signal intensity within the caudate nucleus were observed between groups.

Discussion

In the present study, the neuropathogenesis associated with infection of neonates by a neurovirulent FIV strain, V1CSF, was found to be viral input titer dependent. Compared to cats infected with a lower viral titer, animals infected with high titers of virus exhibited greater developmental impairment concurrent with increased evidence of neuronal injury, including decreased NAA/Cr, increased TMA/Cr, and increased T2-weighted MR image intensities accompanied by cortical atrophy. These *in vivo* changes were supported by *ex vivo* experiments demonstrating titer-dependent expression of putative neurotoxins by FIV-infected feline MDM and neuropathological evidence of neuronal injury

and stress together with accompanying neuroinflammation. Furthermore, neurological impairment was accompanied by systemic abnormalities, including decreased weight gain and greater CD4+ cell depletion, that also varied with input titer. Taken together, these findings indicate that early viral loads in neonatal brain profoundly influence the severity of neurological damage that develops as infection progresses. Moreover, factors that influence viral replication and viral burden, such as the integrity of the host immune response, contribute to these processes.

The present study extends the findings of an earlier report from our laboratory in which neonatal cats infected with V1CSF experienced neurodevelopmental impairment concurrent with a decrease in brain NAA/Cr (Power *et al*, 1998) by demonstrating that both of these properties are dependent on input viral titer. Although decreased NAA levels are associated with neuronal injury and loss (Chong *et al*, 1994; Meyerhoff *et al*, 1993), as with the earlier study, neuronal loss was not apparent in V1CSF-infected neonates *in vivo* despite abundant neuronal death in *ex vivo* neurotoxicity assays. Other studies indicate neuronal dysfunction is associated with a greater reduction in NAA levels than that in situations of overt neuronal loss (De Stefano *et al*, 1995; Jenkins *et al*, 2000; Tracey *et al*, 1997). Because loss of neurons is a feature of adult FIV-infected cats (Meeker *et al*, 1997; Power *et al*, 1997), these findings may indicate that neurons within the developing nervous system are more susceptible to injury leading to functional impairment, but are less likely to die. In support of this concept, levels of TMA-containing metabolites, which have been proposed as a marker of membrane structural damage (Kugel *et al*, 1998), and expression of *c-fos*, a transcription factor shown to be upregulated in response to brain injury and excitotoxic insult (Ferrer *et al*, 2000; Griffiths *et al*, 1997), were also elevated in infected animals in a titer-dependent manner. In addition, neuronal damage that manifested as dysmorphic cell bodies and truncated cellular processes was also more prominent in brain tissue from animals infected with high titers of V1CSF.

Functional impairment of neurons in the absence of cell death may also indicate that several different mechanisms contribute to the neurobehavioral phenotype observed in lentivirus infections. The neuronal injury and death associated with lentiviral infection has been postulated to involve an excitotoxic mechanism that results in increased release of glutamate, an excitatory amino acid neurotransmitter, and subsequent excess excitation of neighboring cells (Power, 2001). Previously, increased glutamate levels were detected concurrent with neuronal loss in adult FIV-infected cats (Power *et al*, 1997), but in the V1CSF-infected neonatal brains in which neuronal loss was not observed, a dose-dependent decrease in glutamate/Cr ratios was observed. A similar phenomenon has been reported in the simian immunodeficiency virus (SIV) model, where limited change in glutamate levels are observed in the CNS early after infection despite elevated plasma levels of the metabolite (Eck *et al*, 1991), but marked increases are detected late in infection (Koutsilieri *et al*, 1999). Thus, neuronal death may be the product of a progressive process that gradually increases glutamate levels to concentrations that are lethal to neurons. In contrast, the neuronal injury that occurs early after infection may result from a glutamate-independent mechanism, such as the FIV-induced increases in TNF-α that have been reported in brain early after infection and concurrent with neuronal damage (Poli *et al*, 1999). The mechanism by which FIV infection results in decreased glutamate in the present study remains unclear, although the observation that this effect was titer dependent suggests that it is a direct result of viral infection. Astrocytes regulate glutamate levels in the brain, and it is conceivable that their ability to take up glutamate is preserved early in infection but declines with disease progression, concurrent with increasing astrocyte cell death (Wesselingh and Thompson, 2001).

The observations that the extent of neuronal loss and brain glutamate levels observed in FIV-infected neonatal kittens differed from that previously reported for adult cats suggest that maturation-dependent host factors contribute to the profile of neurological disease in lentiviral infections. In further support of this concept, increased T2-weighted MRI signal intensities and elevated metabolite levels, evidence of neuropathology and blood-brain barrier (BBB) pertubation (Lanens *et al*, 1993), were detected in frontal white matter and cortex among high titer-infected animals compared to controls, but not in the caudate nucleus. Since neuronal damage in the basal ganglia is observed in adult FIV-infected animals (Power *et al*, 1997), the relative paucity of changes in the caudate nucleus supports the concept that both progressive and acute damage occurs in FIV infected cats, resulting in a different disease profile in neonates and adult animals (Hurtrel *et al*, 1992). The failure to detect viral RNA in necropsied brain tissue from some infected neonates, despite the presence of viral DNA, is also likely a product of age. For example, studies of SIV-infected neonatal macaques found fewer infected cells and sporadic detection of viral RNA in neonatal brain tissue compared to adult subjects, despite comparable prevalence of CNS infection and peripheral viral loads (Westmoreland *et al*, 1999). It is conceivable that the greater plasticity inherent to neonatal brain tissue compared to adult brain contributes to the observed maturation-dependent effects. This property may also promote increased passive migration of virus within the brain, accounting for the comparable levels of virus and neuropathological damage observed in both the implanted and non-implanted hemispheres of infected neonates.

The current results also re-enforce the important role played by systemic factors, such as immune suppression, in FIV-mediated neurological disease. A recent study has reported that both the immunological and neurological disease caused by another neurovirulent FIV strain, PPR, is dose-dependent (Hokanson *et al*, 2000). Similarly, V1CSF induced a titer-dependent depletion of CD4+ cells, while immune suppression with cyclosporin A has been shown to increase the neurovirulence exhibited by a less neurovirulent FIV strain, Petaluma (Power *et al*, 1998). This correlation between immune status and the development of neurological impairment following FIV infection may reflect the relative ability of the host immune response to clear the virus from the CNS. Moreover, such impairment of the developing immune system may have enhanced spread of the virus from the CNS into the systemic circulation, contributing to the colonization of the non-implanted hemisphere of the brain. In light of the capacity for decreased immune function to alter viral phenotype, the findings presented in the current study may also provide insight into the factors that contribute to the strain dependence associated with FIV-induced neurological damage. For both FIV and primate lentiviruses, specific envelope sequences have been shown to confer a neurovirulent phenotype (Bragg *et al*, 1999; Mankowski *et al*, 1997; Power *et al*, 1995). Since brain entry of lentiviruses is thought to involve crossing of the BBB by infected hematogenous cells (Power, 2001) such as monocytes and lymphocytes, and certain lentivirus envelope regions implicated in neurovirulence have also been shown to influence cell tropism (Chesebro *et al*, 1992; Johnston *et al*, 2002; Mankowski *et al*, 1997; Vahlenkamp *et al*, 1999), specific envelope sequences may increase the efficiency with which FIV colonizes the CNS. Thus higher viral loads may be achieved in the CNS, leading to increased neurological damage.

These experiments indicate that the initial dose of virus received by neonatal kittens directly influences the severity of the ensuing neurological and systemic disease following FIV infection. Our findings are consistent with those obtained from the SIV animal model, in which infection of neonatal macaques produced similar neuropathological changes (Westmoreland *et al*, 1999). Moreover, as with FIV, the neurological damage caused by neurovirulent SIV strains occurs rapidly following exposure to the virus (Gonzalez *et al*, 2000) and is associated with limited viral replication in the brain (Westmoreland *et al*, 1999). Despite these similarities, input virus titer and inoculation route has not been found to influence disease outcome in SIV-infected macaques (Westmoreland *et al*, 1998). Although this discrepancy may indicate a fundamental difference in the pathogenesis of FIV and SIV, it more likely reflects the fact that juvenile and adult macaques, not neonates, were investigated in the earlier study. Thus, the results presented here furnish support for early therapeutic intervention to suppress viral load in the brain during lentiviral infections and provide a model for examining the neuropathogenesis of lentiviruses in the developing nervous system.

Methods and materials

Viruses and cell culture

PBMC were isolated from blood obtained from specific pathogen–free (SPF) adult felines by density-gradient centrifugation, as described previously (Johnston and Power, 1999). PBMC were initially stimulated for 3 days with concanavalin A (5 μg/ml, Sigma, Oakville, Ontario), then maintained in RPMI 1640 medium with 15% fetal calf serum (FCS) and interleukin-2 (100 IU/ml, Sigma). Primary monocyte-derived macrophages (MDM) were isolated from unstimulated PBMC by adherence on polystyrene flasks for 24 h, differentiated for 7 days, and cultured in RPMI 1640 medium containing 20% FCS. NG-108 mouse neuroblastoma cells were obtained from American Type Culture Collection (Rockville, MD) and cultured in minimum essential medium (MEM) containing 10% FCS. All cell cultures were supplemented with 1% penicillin and streptomycin. The primary FIV isolate, V1CSF, which was derived from the CSF of a cat with encephalopathy and shown previously to possess a neurovirulent phenotype (Power *et al*, 1998). Viral stocks were prepared in primary feline PBMC and underwent fewer than 10 passages prior to the present experiments. Viral titers were determined by limiting dilution in feline PBMC and RT assay, as described previously (Lanens *et al*, 1993). For infection, MDM were inoculated with 200 μl of viral stock ($10^{2.5}$ or $10^{4.5}$ $TCID_{50}$/ml), incubated for 2 h at 37°C, washed twice, and cultured in AIM V serum-free medium (Gibco, Burlington, Ontario) until supernatants and cells were harvested. Uninfected cells or mock-infected cells treated with heat-inactivated virus served as controls.

Neurotoxicity assay

NG-108 neuroblastoma cells (5×10^4/well) were seeded in 96-well plates in AIM V medium and differentiated by incubation with 1 mM dibutyryl cAMP (Sigma, Oakville, Ontario) for 24 h to induce a neuronal phenotype (Ghahary *et al*, 1989). Differentiated neurons were incubated for 24 h with CM harvested at days 1 and 3 PI from mock- and V1CSF-infected feline MDM. These time points were selected based on previous experiments demonstrating that the neurotoxicity induced by V1CSF reaches its peak value before day 4 PI (Power *et al*, 1998). Following exposure to CM, cultures were stained with trypan blue dye for 15 min at room temperature and the number of cells, which failed to exclude the dye, were counted in four wells (three to six fields per well, 0.1 mm^2 per field) by an observer unaware of the

treatment identity. Neuronal death was expressed as the mean percentage ± SEM of stained cells compared to the total number of counted cells (equalized to control values). A consistent level of background cell death (3% to 5%) was observed between experiments.

Animals and virus inoculation

SPF pregnant cats (queens) were obtained from Unique Ventures (Winnipeg, Manitoba, Canada) and housed according to University of Calgary Animal Resource Center guidelines. All queens were found to be negative for feline retroviruses by PCR analysis and serological testing. At day 1 post delivery, neonatal kittens were inoculated intracranially (right frontal lobe) with 0.2 ml of either $10^{2.5}$ (low-titer, $n = 4$) or $10^{4.5}$ (high-titer, $n = 6$) $TCID_{50}$/ml of infectious V1CSF or heat-inactivated virus using a 30-gauge needle and syringe. Mock-infected animals inoculated with heat-inactivated V1CSF ($n = 7$) served as controls. Each experimental group was comprised of at least two litters from different queens. Kittens, weaned at 6 weeks, were monitored weekly for changes in body weight and neurodevelopmental impairment. PBMC were isolated from blood collected at 8 and 12 weeks PI for flow cytometry analysis of CD4+ and CD8+ cell levels. After 12 weeks, animals were euthanized and brain and spleen tissues were harvested. Samples from each animal were fixed in 4% buffered (pH 7.1) paraformaldehyde (PFA) or frozen immediately by immersion in liquid nitrogen for immunocytochemical and PCR analyses, respectively.

Neurodevelopmental studies

To assess the development of neurological disease, FIV- and mock-infected kittens were examined weekly by animal care staff unaware of their infection status and the age at which animals were able to successfully complete specific neurodevelopmental tasks (running, jumping, air righting, plank walking, and blink reflex) was determined. Neurodevelopmental impairment was expressed as a MDS score (Heseltine *et al*, 1998), for which values between 0.5 and 1.0 indicate normal neurobehavioral development. These scores were calculated based on results obtained between weeks 6 and 12 PI and represented the mean number of standard deviations by which animals in each group differed from previous control values (Power *et al*, 1998).

Flow cytometry

PBMC were isolated from whole blood, as described above, and aliquots of 1×10^6 cells were resuspended in phosphate-buffered saline (PBS) containing 0.1% sodium azide. Resuspended cells were incubated for 20 min at room temperature with 3 μg of anti-CD4 or -CD8 monoclonal antibodies per milliliter (clones FE1.7B12 and FE1.10E9; LABL, Davis, California), washed twice with PBS, and incubated for 20 min with fluorescein thiocyanate (FITC)-conjugated goat anti-mouse IgG (0.25 μg/μl; Becton Dickinson, San Jose, California). PBMC were again washed, then resuspended in 0.5 ml of 1% formalin in PBS for analysis. Using a FacScan flow cytometer (Becton Dickinson) with the argon laser excitation set at 488 nm, data were collected from approximately 15,000 events for each experimental condition and results were expressed as a single-parameter log fluorescence histogram. Cells incubated in the absence of antibodies or with 1 μg/ml of FITC-labeled, isotype-matched murine immunoglobulin G_1 (IgG_1) (Becton Dickinson) served as controls.

Immunocytochemistry

PFA-fixed necropsied brain tissue was cryoprotected by immersion in 30% sucrose for 3 days. Because earlier studies (Power *et al*, 1997, 1998) indicated no differences in severity of neuropathology between implanted and nonimplanted hemispheres, we focused these studies on the nonimplanted hemisphere. Serial free-floating (30-μm) sections (frontal cortex and white matter) were prepared using a sliding microtome and stored at 4°C in PBS containing 0.04% sodium azide. In preparation for use, sections were washed with PBS, then incubated for 30 min at room temperature in 3% hydrogen peroxide. Sections were washed again and incubated for 45 min at room temperature in blocking solution containing 10% normal goat serum (NGS, Sigma) and 0.4% Triton X-100 in PBS. Following the blocking step, sections were incubated for 24 to 48 h with primary antibody diluted in PBS containing 5% NGS and 0.4% Triton X-100, washed, and incubated for 2 h with secondary antibody diluted in PBS containing 1.5% NGS. Primary antibodies used for these studies included (1:5,000; DAKO Diagnostics, Mississauga, Ontario), *c-fos* (1:10,000; Oncogene Research Products, Boston, MA), MAP-2 (1:5,000; Sigma), and CD18 (1:100; provided by Dr. Peter Moore, University of California, Davis, CA). Monoclonal and polyclonal antibodies were detected using horseradish peroxidase (HRP)-conjugated goat anti-mouse (Jackson ImmunoResearch Lab) or anti-rabbit (Sigma) secondary antibodies, respectively, and visualized by incubation with diaminobenzidine and hydrogen peroxide.

Detection of virus

Total cellular RNA was isolated using TRIzol reagent (Gibco), DNase-treated (1 U/μg) for 1 h at 37°C, and the absence of contaminating cellular DNA was confirmed by PCR using the conditions and primers described below. cDNA was prepared from 100 ng of treated RNA using a First Strand cDNA Synthesis kit (Boehringer-Mannheim, Quebec) with a poly(dT) primer alone or in combination with a primer targeting a specific gene. Genomic DNA was isolated using DNAzol reagent (Gibco). Approximately 300 to 400 ng of template DNA or cDNA was amplified by 1 cycle of 95°C for 5 min, 30 cycles of 95°C for

1 min, 50°C for 1 min, and 72°C for 2 min, and 1 cycle of 72°C for 10 min. Nested PCR was performed using 2 μl of product amplified in the first PCR reaction at an annealing temperature of 55°C. To minimize the possibility of contamination, PCR reactions were prepared in three separate rooms and control sample were used in which 2 μl of water was added to the reaction mixture instead of template. Loading of equal amounts of template from each sample was ensured by semiquantitative amplification of the host gene, glyceraldehyde-3-phosphate dehydrogenase (GAPDH), at an annealing temperature of 55°C. The sequences of all primers were reported previously (Johnston *et al*, 2000). PCR products were separated by agarose gel electrophoresis and amplification of a single band of the correct molecular weight was determined by ethidium bromide staining.

Spectroscopy and imaging

In vivo MR spectroscopy was performed on mock- and FIV-infected animals, as described previously (Power *et al*, 1998). Briefly, animals were anesthetized at week 12 PI and localized proton (^{1}H) MR spectra were obtained from volumes of 64 μl of the left frontal cortex and caudate nucleus using STEAM localization. A total of 512 signal averages were acquired (acquisition time 17.1 min per spectrum) using a 7-T 21-cm Bruker/Biospec2 spectrometer and a 4-cm diameter circular surface coil from the nonimplanted hemisphere. Spectra were processed by apodizing with a 15-Hz exponential multiplication, Fourier transformation, phasing, and modest polynomial baseline correction. Peak intensities were measured and metabolite ratios were expressed relative to the stable total creatine signal (Prichard and Shulman, 1986). High resolution ^{1}H MR spectroscopy was performed on frozen brain tissue (left frontal cortex), collected at necroscropy as described above, following extraction in perchloric acid, neutralization, chelation, and pH adjustment (Power *et al*, 1997). Spectra were obtained at 500 MHz (11.7 T) using a Bruker AMX-500 spectrometer locked to the D_2O deuterium resonance and the peaks of major brain metabolites were assigned based on previously published spectra. Metabolite concentrations were determined by comparing the integrated intensities of the assigned peaks to the intensity of the peak of a known amount of a sodium-d_4-(trimethylsilyl)propionate (TMS) standard, after correcting for the dry tissue weight, and expressed relative to creatine levels in each sample. T2-weighted MR imaging was performed on infected (Six high-titer, three low-titer) and control ($n = 6$) animals as described previously (Lei *et al*, 1998) using a 4 cm × 4 cm coil and a standard spin-echo technique with an echo time of 75 ms. A total of five measurements were averaged for each region and equalized to the T2-values of facial muscle for each subject.

Statistical analyses

Statistical analyses were performed using Graphpad Prism (Graphpad Software, San Diego, CA). For comparisons of three or more unmatched groups, one-way analysis of variance (ANOVA) was performed followed by Tukey-Kramer multiple-comparison post hoc tests to determine differences between specific groups. For data derived from two groups, a Student's *t* test was used. *P* values of less than .05 were considered significant for all tests.

References

Bendinelli M, Pistello M, Lombardi S, Poli A, Garzelli C, Matteucci D, Ceccherini-Nelli L, Malvaldi G, Tozzini F (1995). Feline immunodeficiency virus: An interesting model for AIDS studies and an important cat pathogen. *Clin Microbiol Rev* **8:** 87–112.

Billaud JN, Selway D, Yu N, Phillips TR (2000). Replication rate of feline immunodeficiency virus in astrocytes is envelope dependent: Implications for glutamate uptake. *Virology* **266:** 180–188.

Boche D, Hurtrel M, Gray F, Claessens-Maire MA, Ganiere JP, Montagnier L, Hurtrel B (1996). Virus load and neuropathology in the FIV model. *J NeuroVirol* **2:** 377–387.

Bragg DC, Meeker RB, Duff BA, English RV, Tompkins MB (1999). Neurotoxicity of FIV and FIV envelope protein in feline cortical cultures. *Brain Res* **816:** 431–437.

Chesebro B, Wehrly K, Nishio J, Perryman S (1992). Macrophage-tropic human immunodeficiency virus isolates from different patients exhibit unusual V3 envelope sequence homogeneity in comparison with T-cell-tropic isolates: Definition of critical amino acids involved in cell tropism. *J Virol* **66:** 6547–6554.

Chong WK, Paley M, Wilkinson ID, Hall-Craggs MA, Sweeney B, Harrison MJ, Miller RF, Kendall BE (1994). Localized cerebral proton MR spectroscopy in HIV infection and AIDS. *AJNR Am J Neuroradiol* **15:** 21–25.

De Stefano N, Matthews PM, Arnold DL (1995). Reversible decreases in *N*-acetylaspartate after acute brain injury. *Magn Reson Med* **34:** 721–727.

Dow SW, Dreitz MJ, Hoover EA (1992). Feline immunodeficiency virus neurotropism: Evidence that astrocytes and microglia are the primary target cells. *Vet Immunol Immunopathol* **35:** 23–35.

Eck HP, Stahl-Hennig C, Hunsmann G, Droge W (1991). Metabolic disorder as early consequence of simian immunodeficiency virus infection in rhesus macaques. *Lancet* **338:** 346–347.

Ferrer I, Lopez E, Blanco R, Rivera R, Krupinski J, Marti E (2000). Differential c-Fos and caspase expression following kainic acid excitotoxicity. *Acta Neuropathol (Berl)* **99:** 245–256.

Ghahary A, Vriend J, Cheng KW (1989). Modification of the indolamine content in neuroblastoma × glioma hybrid NG108-15 cells upon induced differentiation. *Cell Mol Neurobiol* **9:** 343–355.

Gonzalez RG, Cheng LL, Westmoreland SV, Sakaie KE, Becerra LR, Lee PL, Masliah E, Lackner AA (2000). Early

brain injury in the SIV-macaque model of AIDS. *Aids* **14:** 2841–2849.

Griffiths R, Malcolm C, Ritchie L, Frandsen A, Schousboe A, Scott M, Rumsby P, Meredith C (1997). Association of c-fos mRNA expression and excitotoxicity in primary cultures of mouse neocortical and cerebellar neurons. *J Neurosci Res* **48:** 533–542.

Gruol DL, Yu N, Parsons KL, Billaud JN, Elder JH, Phillips TR (1998). Neurotoxic effects of feline immunodeficiency virus, FIV-PPR. *J NeuroVirol* **4:** 415–425.

Heseltine PN, Goodkin K, Atkinson JH, Vitiello B, Rochon J, Heaton RK, Eaton EM, Wilkie FL, Sobel E, Brown SJ, Feaster D, Schneider L, Goldschmidts WL, Stover ES (1998). Randomized double-blind placebo-controlled trial of peptide T for HIV-associated cognitive impairment. *Arch Neurol* **55:** 41–51.

Hokanson RM, TerWee J, Choi IS, Coates J, Dean H, Reddy DN, Wolf AM, Collisson EW (2000). Dose response studies of acute feline immunodeficiency virus PPR strain infection in cats. *Vet Microbiol* **76:** 311–327.

Hurtrel M, Ganiere JP, Guelfi JF, Chakrabarti L, Maire MA, Gray F, Montagnier L, Hurtrel B (1992). Comparison of early and late feline immunodeficiency virus encephalopathies. *Aids* **6:** 399–406.

Jenkins BG, Klivenyi P, Kustermann E, Andreassen OA, Ferrante RJ, Rosen BR, Beal MF (2000). Nonlinear decrease over time in *N*-acetyl aspartate levels in the absence of neuronal loss and increases in glutamine and glucose in transgenic Huntington's disease mice. *J Neurochem* **74:** 2108–2119.

Johnston JB, Jiang Y, van Marle G, Mayne MB, Ni W, Holden J, McArthur JC, Power C (2000). Lentivirus infection in the brain induces matrix metalloproteinase expression: Role of envelope diversity. *J Virol* **74:** 7211–7220.

Johnston JB, Power C (1999). Productive infection of human peripheral blood mononuclear cells by feline immunodeficiency virus: Implications for vector development. *J Virol* **73:** 2491–2498.

Johnston JB, Silva C, Power C (2002). Envelope gene-mediated neurovirulence in feline immunodeficiency virus infection: Induction of matrix metalloproteinases and neuronal injury. *J Virol* **76:** 2622–2633.

Koutsilieri E, Sopper S, Heinemann T, Scheller C, Lan J, Stahl-Hennig C, ter Meulen V, Riederer P, Gerlach M (1999). Involvement of microglia in cerebrospinal fluid glutamate increase in SIV-infected rhesus monkeys (Macaca mulatta). *AIDS Res Hum Retroviruses* **15:** 471–477.

Kugel H, Heindel W, Roth B, Ernst S, Lackner K (1998). Proton MR spectroscopy in infants with cerebral energy deficiency due to hypoxia and metabolic disorders. *Acta Radiol* **39:** 701–710.

Lanens D, Spanoghe M, Van Audekerke J, Van der Linden A, Dommisse R (1993). Complementary use of T2- and postcontrast T1-weighted NMR images for the sequential monitoring of focal ischemic lesions in the rat brain. *Magn Reson Imaging* **11:** 675–683.

Lei H, Dooley P, Peeling J, Corbett D (1998). Temporal profile of magnetic resonance imaging changes following forebrain ischemia in the gerbil. *Neurosci Lett* **257:** 105–108.

Mankowski JL, Flaherty MT, Spelman JP, Hauer DA, Didier PJ, Amedee AM, Murphey-Corb M, Kirstein LM, Munoz A, Clements JE, Zink MC (1997). Pathogenesis of simian immunodeficiency virus encephalitis: Viral determinants of neurovirulence. *J Virol* **71:** 6055–6060.

McArthur JC (1987). Neurologic manifestations of AIDS. *Medicine (Baltimore)* **66:** 407–437.

McArthur JC, McClernon DR, Cronin MF, Nance-Sproson TE, Saah AJ, St Clair M, Lanier ER (1997). Relationship between human immunodeficiency virus-associated dementia and viral load in cerebrospinal fluid and brain. *Ann Neurol* **42:** 689–698.

Meeker RB, Thiede BA, Hall C, English R, Tompkins M (1997). Cortical cell loss in asymptomatic cats experimentally infected with feline immunodeficiency virus. *AIDS Res Hum Retroviruses* **13:** 1131–1140.

Meyerhoff DJ, MacKay S, Bachman L, Poole N, Dillon WP, Weiner MW, Fein G (1993). Reduced brain *N*-acetylaspartate suggests neuronal loss in cognitively impaired human immunodeficiency virus-seropositive individuals: In vivo ^{1}H magnetic resonance spectroscopic imaging. *Neurology* **43:** 509–515.

Phillips TR, Prospero-Garcia O, Puaoi DL, Lerner DL, Fox HS, Olmsted RA, Bloom FE, Henriksen SJ, Elder JH (1994). Neurological abnormalities associated with feline immunodeficiency virus infection. *J Gen Virol* **75:** 979–987.

Podell M, March PA, Buck WR, Mathes LE (2000). The feline model of neuroAIDS: Understanding the progression towards AIDS dementia. *J Psychopharmacol* **14:** 205–213.

Podell M, Hayes K, Oglesbee M, Mathes L (1997). Progressive encephalopathy associated with CD4/CD8 inversion in adult FIV-infected cats. *J Acquir Immune Defic Syndr Hum Retrovirol* **15:** 332–340.

Poli A, Pistello M, Carli MA, Abramo F, Mancuso G, Nicoletti E, Bendinelli M (1999). Tumor necrosis factor-alpha and virus expression in the central nervous system of cats infected with feline immunodeficiency virus. *J NeuroVirol* **5:** 465–473.

Power C (2001). Retroviral diseases of the nervous system: Pathogenic host response or viral gene-mediated neurovirulence? *Trends Neurosci* **24:** 162–169.

Power C, Buist R, Johnston JB, Del Bigio MR, Ni W, Dawood MR, Peeling J (1998). Neurovirulence in feline immunodeficiency virus-infected neonatal cats is viral strain specific and dependent on systemic immune suppression. *J Virol* **72:** 9109–9115.

Power C, McArthur JC, Johnson RT, Griffin DE, Glass JD, Dewey R, Chesebro B (1995). Distinct HIV-1 env sequences are associated with neurotropism and neurovirulence. *Curr Top Microbiol Immunol* **202:** 89–104.

Power C, Moench T, Peeling J, Kong PA, Langelier T (1997). Feline immunodeficiency virus causes increased glutamate levels and neuronal loss in brain. *Neuroscience* **77:** 1175–1185.

Prichard JW, Shulman RG (1986). NMR spectroscopy of brain metabolism in vivo. *Annu Rev Neurosci* **9:** 61–85.

Tracey I, Lane J, Chang I, Navia B, Lackner A, Gonzalez RG (1997). ^{1}H magnetic resonance spectroscopy reveals neuronal injury in a simian immunodeficiency virus macaque model. *J Acquir Immune Defic Syndr Hum Retrovirol* **15:** 21–27.

Vahlenkamp TW, de Ronde A, Schuurman NN, van Vliet AL, van Drunen J, Horzinek MC, Egberink HF (1999). Envelope gene sequences encoding variable re-

gions 3 and 4 are involved in macrophage tropism of feline immunodeficiency virus. *J Gen Virol* **80:** 2639–2646.

Wesselingh SL, Thompson KA (2001). Immunopathogenesis of HIV-associated dementia. *Curr Opin Neurol* **14:** 375–379.

Westmoreland SV, Halpern E, Lackner AA (1998). Simian immunodeficiency virus encephalitis in rhesus macaques is associated with rapid disease progression. *J NeuroVirol* **4:** 260–268.

Westmoreland SV, Williams KC, Simon MA, Bahn ME, Rullkoetter AE, Elliott MW, deBakker CD, Knight HL, Lackner AA (1999). Neuropathogenesis of simian immunodeficiency virus in neonatal rhesus racaques. *Am J Pathol* **4:** 1217–1228.

Yu N, Billaud JN, Phillips TR (1998). Effects of feline immunodeficiency virus on astrocyte glutamate uptake: Implications for lentivirus-induced central nervous system diseases. *Proc Natl Acad Sci USA* **95:** 2624–2629.

Zenger E, Tiffany-Castiglioni E, Collisson EW (1997). Cellular mechanisms of feline immunodeficiency virus (FIV)-induced neuropathogenesis. *Front Biosci* **2:** d527–d537.

Zink MC, Suryanarayana K, Mankowski JL, Shen A, Piatak M, Jr, Spelman JP, Carter DL, Adams RJ, Lifson JD, Clements JE (1999). High viral load in the cerebrospinal fluid and brain correlates with severity of simian immunodeficiency virus encephalitis. *J Virol* **73:** 10480–10488.